ASTRON 120 Lab 3 Report - Exoplanet Transit

Quentin Le Ny
UC Berkeley
Department of Astronomy
quentin.le.ny@berkeley.edu
Group 3
Quentin Le Ny, Kobe Bilstad, Brianna Peck

November 5, 2024

Abstract

The lab results discussed in this report focus on the transit observations of a known exoplanet, named "TOI-2154 b". The observations were taken on the night of October 17-18th, 2024, from 9:51pm to 1:00am. Despite the interference from the moon's luminosity at 99% of maximum and mild cloud cover, we were able to maintain a Full Width at Half Maximum value of approximately 5.00 throughout the collection of images. Due to initial difficulties in achieving precise telescope pointing, manual adjustments to the right ascension and declination were required based on the first identification of stellar positions to ensure the telescope remained aligned with the target, cross-correlated with the Airmass.org Field of View. Despite these challenges, we successfully recorded over three-quarters of the transit event. Unfortunately, we were left with no choice but to equate our egress duration with our ingress duration. Now, due to the shift in the star's position in our telescopes field of view, along with neighboring stars, we then performed a robust alignment and cleaning of our images. Recording the flux from our star as it moved along the night sky, we were able to produce a light curve (luminosity vs. time) Through thorough analysis and approximal methods, we determined four observables - transit and ingress/egress duration, and transit depth. They were approximated to be, respectively: $155 \pm 5.50, 30 \pm 3.89, 30 \pm 3.89, 10.36\% \pm 0.86\%$. This report will use these observables to calculate the specifications of our transiting planet, and compare them with a 2023 report on TOI-2154b. (7)

1 Introduction

Growth in the discovery of exoplanets has been exponential in the last decade, particularly with the emergence and refinement of the "transit" method, first used to confirm the existence of an exoplanet in 1999. [1] This method aims at observing the light flux emitted by stars over periods of time, and looking for any abnormal, sustained dips in flux. Now, these dips could indicate a variety of different flux-obstructing sources: dust clouds, binary stars, or perhaps giant alien rockets! In this particular report however, the focus of its flux observations will be to detect transiting planets, ruling out the possibility of any other interstellar object which could potentially be blocking star light. Exoplanets, or any massive object in a stable orbit around a star, will orbit at a constant velocity, and transit a star for a given, constant amount of time. This in turn, along with the reduction in recorded flux from the star, gives us a great deal of information about the star and its system: the radii and mass of the star and its planet (and

thus their densities), and the planet's orbital period, eccentricity, and radius. Although this report only makes use of data during one transit, subsequent observations will confirm the recurring nature of the orbit of the planet of interest, which is typically confirmed after 3 successful, well constrained observations of a transit.

2 Methods & Observations

Located at the Russell Reservation in California, Leuschner Observatory is home to a 30-inch telescope, which is useful to numerous educational astronomical studies for undergraduates at UC Berkeley. You'll see a fairly close up image of the telescope on the right. This telescope is equipped with an SBIG STL-11000M-C1 CCD camera, featuring a 4008 $\times$ 2672 pixel array, which translates into a field of view of approximately 20 $\times$ 13.4 arc minutes. The pixel scale is finely set at 0.335 arcseconds per pixel without binning, ideal for precise celestial observations.

Historically, Leuschner Observatory has been a pivotal facility for educational and research purposes in astronomy. It offers hands-on experience to students and is instrumental in gathering significant observational data. The observatory's location and technological setup are designed to minimize light pollution while maximizing the quality and quantity of astronomical data that can be collected.

For our astrophysics lab, the observatory's telescope is particularly well-suited due to its high-resolution CCD camera and the ability to use a binning factor of 2. This reduces readout noise and overheads without under-sampling the full width at half maximum (FWHM) of stars, crucial for observing the subtle dimming caused by transiting exoplanets. The facility also supports various calibration frames like bias, darks, and flats, ensuring that data are accurately corrected for instrumental effects, making it an excellent tool for detecting and studying exoplanets like TOI-2154 b.

Figure 1: Leuschner Telescope

2.1 Selecting Transiting Planet

The selection process for identifying an appropriate transiting exoplanet to observe involved parsing through the Swarthmore Exoplanet Database. Utilizing a Jupyter notebook, we employed Python libraries such as Pandas to manipulate and filter the data effectively. The dataset included critical parameters such as right ascension, declination, visual magnitude, period, and depth of transit.

Initially, we set stringent criteria to isolate potential candidates that met specific observational constraints conducive to our lab setup. These constraints included:

- Visual magnitude between 8 and 11.5, ensuring the targets were neither too dim nor excessively bright to minimize integration time, (the lower the integration time, the more refined our flux data will be).
- Transit duration of ≤ 3 hours, to fit within our limited nightly observation window.
- Transit depth of at least 10%, to ensure detectable changes in brightness.

After applying these filters, we found several candidates. Initially, WASP-33b appeared optimally suitable. However, due to unforeseen poor weather conditions on the observation night of October 12, 2024, observing WASP-33b became unfeasible.

As a result, we selected TOI-2154 b, the next best option. This decision ensured that we could conduct meaningful observations without interruption, adhering to the project timeline and objectives.

	name	RA	Dec	vmag	period	duration	depth
0	Gaia-2 b	07:22:56.48	+67:15:09.56	11.3	3.691522	2.72	16.3
1	HAT-P-20 b	07:27:39.94	+24:20:10.03	11.2	2.875318	1.61	23.7
2	HAT-P-22 b	10:22:43.55	+50:07:43.36	9.8	3.212230	2.65	14.4
3	HAT-P-30 b	08:15:47.96	+05:50:12.72	10.4	2.810601	2.13	13.0
4	HAT-P-56 b	06:43:23.52	+27:15:07.86	10.9	2.790825	2.27	11.0
5	Qatar-6 b	14:48:50.42	+22:09:09.41	11.5	3.506165	1.60	18.4
6	TOI-2154 b	04:44:06.76	+84:21:51.35	11.1	3.824083	2.52	10.1
7	WASP-14 b	14:33:06.39	+21:53:40.87	9.7	2.243766	2.57	10.0
8	WASP-33 b	02:26:51.06	+37:33:01.60	8.1	1.219871	2.85	12.2
9	WASP-49 b	06:04:21.53	-16:57:55.40	11.4	2.781737	2.14	14.0
10	WASP-50 b	02:54:45.14	-10:53:52.89	11.4	1.955092	1.83	19.6
11	WASP-77 A b	02:28:37.33	-07:03:38.40	10.3	1.360029	2.15	17.8
12	WASP-84 b	08:44:25.68	+01:51:35.62	10.8	8.523496	2.76	17.2
13	WASP-85 A b	11:43:37.93	+06:33:49.62	10.7	2.655674	2.60	18.7
14	XO-2 N b	07:48:06.42	+50:13:30.53	11.2	2.615859	2.68	13.4
15	XO-6 b	06:19:10.31	+73:49:39.24	10.2	3.764995	2.64	14.7

Figure 2: Suitable Candidates for Transit Observations

Figure 3 below shows the airmass.org plot for the planet's transit duration, highlighted in light green, with its elevation (in degrees) relative to our observational location, plotted against time as a straight line. The dotted line represents the moon's trajectory.

The plot underneath that shows the field of view, at 14.81' arcminutes, taken from the website Aladin (Lite). You will see in section 2.2, although with much less focus, that it aligns with our image of a similar field of a view in the sky, after image cleaning.

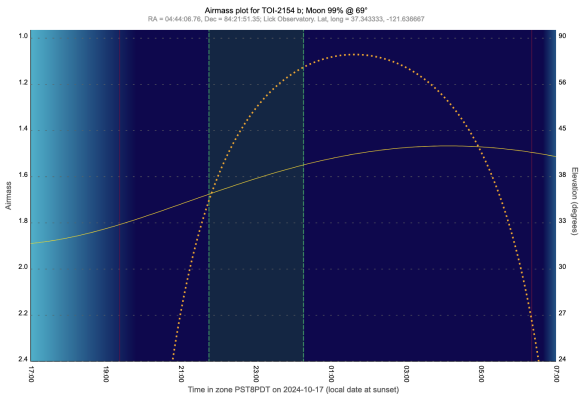

Figure 3: Transiting Planet Range and Path on 10/17

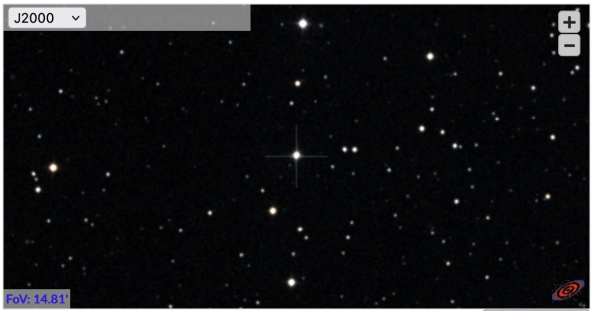

Figure 4: Aladin Field of View of TOI-254

2.2 Observations and Image Cleaning

To minimize noise in our images, we followed a process entailing the creation of master frames (images created from averaging multiple calibration frames) for bias, dark, and flat fields to correct for pixel-to-pixel sensitivity variations and to mitigate dark current noise. Each observational image underwent calibration using these master frames by subtracting the master bias and dark frames, and then normalizing with the master flat frame.

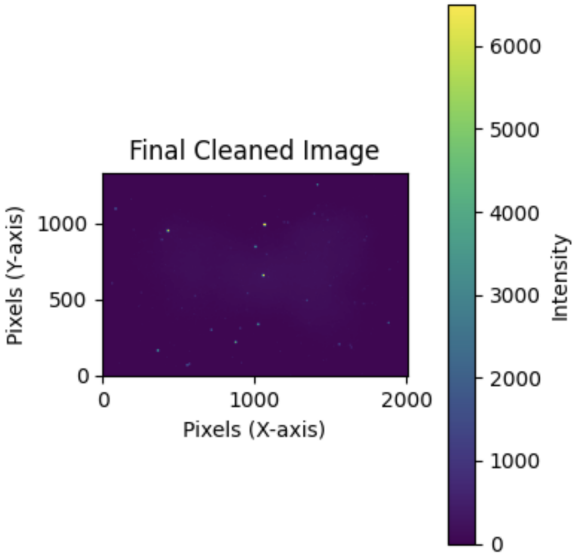

Figure 5: Final Cleaned Image

Figure 6 thus illustrates the cleaned image with apertures placed around each detected flux point. These apertures are critical for comparing the flux of the target star against that of multiple reference stars within the same field of view. Selecting appropriate reference stars ensures the flux stability necessary for accurate transit detection. This method helps to mitigate variations caused by atmospheric conditions or instrumental factors, thereby stabilizing the light curve data used to analyze the transiting exoplanet.

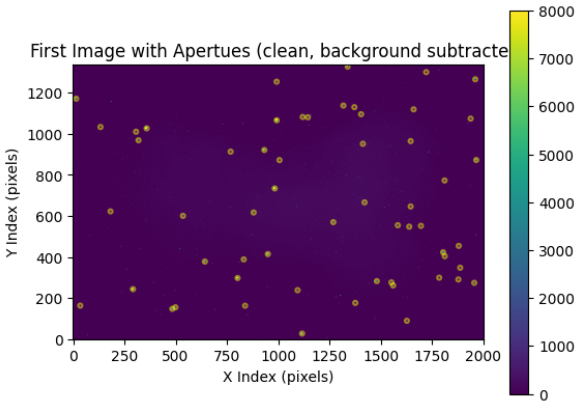

Figure 6: Star Apertures in Cleaned Image

3 Data Processing

In this section, we focus on processing the cleaned and calibrated images to generate a light curve for our target star. The curve will measure and plot the stellar brightness over time, which involves aligning images, calibrating flux values from neighboring stars, and extracting measurements from the apertures around our target star. These measurements will serve as the basis for calculating the physical characteristics of the transiting exoplanet in Section 4.

3.1 Image Alignment

Image alignment is essential for ensuring consistent star positions across frames. This process corrects for drifts by measuring pixel shifts between images. Mathematically, we compute cross-correlation between a reference image and each subsequent image to detect shifts. These shifts are then adjusted to align all images, ensuring that flux measurements reflect actual stellar variations rather than positional discrepancies.

3.2 Flux Calibration from Neighboring Stars

Flux calibration is conducted using flux measurements from neighboring (reference) stars. By employing differential photometry techniques, Python scripts analyze the flux collected through each aperture and identify the top five brightest stars (assisted by the apertures in Figure 6). These stars serve as reference points for calibrating the flux of the target star, ensuring that the light curve reflects intrinsic brightness changes due to the exoplanet transit, free from atmospheric, stellar, and instrumental variations.

3.3 Creating Light Curve

The light curve is constructed by plotting the calibrated flux of the target star over time, using data from aligned and calibrated images. Flux values are plotted against the time of each observation, illustrating the brightness variations of the star as the exoplanet transits in front of it. Error bars in the light curve are determined based on the standard deviation of the flux measurements from the reference stars, providing an estimate of the uncertainty in each flux value over the observation period.

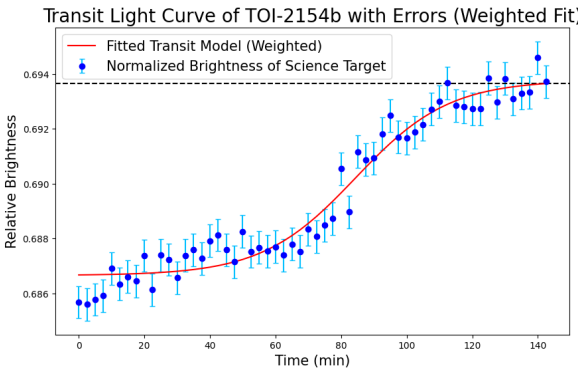

Figure 7: Light Curve

3.4 Obtaining Observable and Uncertainty Values from Curve

To extract observables such as the transit duration and depth from the light curve, we employ statistical techniques, given the partial observation of the transit. We calculate the average of the highest uncertainties within the error bars during the observed transit phase. This average serves as a threshold to determine the onset of the egress. Specifically, when the midpoint of a flux measurement's uncertainty surpasses this average, we infer the start of egress. However, the end of the egress phase had to be approximated visually.

4 Results

In this section, we utilize the observables extracted from the light curve. We derive the planet's orbital characteristics, such as orbital period and semi-major axis, directly from our observations. The radius of the star and mass of the planet is sourced from external databases to facilitate these calculations. The orbital eccentricity is assumed to be zero, since we must assume ingress duration to equal egress duration to avoid complicating calculations. We will then compare our findings with previous studies to assess consistency and accuracy.

4.1 Observables, Precision Check

The observed values for TOI-2154 b closely align with expectations, considering typical error margins in transit photometry. The transit duration deviates slightly from expectations. Ingress/egress durations recorded a -7.9% error, well within the acceptable range for astronomical observations. The transit depth error at +10.3% is slightly above average, but acceptable in exoplanet transit studies, where complexities such as atmospheric properties can affect depth measurements. Overall, these results confirm the reliability of our observational setup and data processing techniques.

	Obs. Vals	Onl. Est.	Onl. Upp. Est.	Onl. Low. Est.	Obs. Est.	Obs. Upp. Est.
1	Transit (mins)	147.9	149.3	146.5	155	160.5
2	Ingress (mins)	27.62	28.56	26.7	30	33.89
3	Egress (mins)	27.62	28.56	26.7	30	33.89
4	Transit Depth	0.01143	0.01163	0.01124	0.01036	0.01229

Figure 8: Online and Observable Values and Uncertainties

	Obs. Vals	Onl. Est.	Obs. Est.	Diff.	% Error
1	Transit (mins)	147.9	155	-7.1	-4.6%
2	Ingress (mins)	27.62	30	-2.381	-7.9%
3	Egress (mins)	27.62	30	-2.381	-7.9%
4	Transit Depth	0.01143	0.01036	0.001068	10.3%

Figure 9: Differences between Online and Observable Values

4.2 Calculations, Precision Check

	Vals	Onl. Est.	E Est.	T Est.
1	R_star	9.716e+08	9.716e+08	9.716e+08
2	R_p	1.016e+08	9.89e+07	9.89e+07
3	M_star	2.452e+30	1.758e+29	6.356e+29
4	M_p	1.746e+27	1.746e+27	1.746e+27
5	V_p	4.391e+24	4.053e+24	4.053e+24
6	ρ_p	370	430.9	430.9
7	v_orb	1.226e+05	1.099e+05	2.089e+05
8	Ψ	0.5942	0.5538	0.5538
9	b	0.8636	0.8505	0.8505
10	P	1.377e+04	5.555e+04	2.922e+04
11	a	7.674e+09	9.716e+08	9.716e+08
12	i	83.37	20.43	20.43

Figure 10: Comparison of Online and Ingress/Transit Calculations

	Vals	Diff. E	% Error E	Diff. T	% Error T
0	R_star	0	0.0%	0	0.0%
1	R_p	2.676e+06	2.6%	2.676e+06	2.6%
2	M_star	2.277e+30	92.8%	1.817e+30	74.1%
3	M_p	0	0.0%	0	0.0%
4	V_p	3.379e+23	7.7%	3.379e+23	7.7%
5	ρ_p	60.86	16.4%	60.86	16.4%
6	v_orb	1.27e+04	10.4%	8.635e+04	70.4%
7	Ψ	0.04039	6.8%	0.04039	6.8%
8	b	0.01308	1.5%	0.01308	1.5%
9	P	4.179e+04	303.5%	1.545e+04	112.2%
10	a	6.703e+09	87.3%	6.703e+09	87.3%
11	i	62.94	75.5%	62.94	75.5%

Figure 11: Discrepancies in Ingress and Transit Calculations

The calculations for transit-related parameters, such as the semi-major axis and orbital period, are sensitive to the method used to determine the orbital velocity. Using it derived from ingress/egress times leads to different values than when calculating it from transit duration. These derivations, sourced from Professor Lu's lecture slides, highlight the complexities of astrophysical measurements and their dependency on the chosen observational and computational approaches.

4.3 Jupiter Radius Comparison

	Parameter	Est.	Upp. Est.	Low. Est.
0	Onl. R_Jupiter	1.451	1.504	1.403
1	Obs. R_Jupiter	1.413	1.593	1.383
2	Onl. vs Obs. Diff	0.03823	-0.08895	0.02039
3	Onl. vs Obs % Error	2.705%	-5.583%	1.474%

Figure 12: Jupiter Comparison with Transit Method Calculations

5 Discussion & Conclusion

This research into the transit of exoplanet TOI-2154 b has significantly enhanced my understanding of its characteristics and underscored the inherent challenges of astrophysical measurements. The particularly frustrating (yet rewarding) observation process faced numerous challenges, including telescope alignment issues and limitations imposed by atmospheric conditions, which reflect the typical challenges of the average astronomer

Despite these complexities, the observations yielded valuable data. While there were discrepancies in measurements such as stellar mass and orbital velocity - reflecting the sensitivity of our results to initial assumptions and measurement precision - the core transit parameters, including the planet's radius and orbital period, were determined with sufficient accuracy. These measurements provide a reliable basis for interpreting a potential POI (planetary object of interest)'s physical characteristics and its orbit around the host star, with relatively low error margins in the transit depth and duration.

The project also served as a profound educational experience, reinforcing the importance of precision and rigor in scientific research. It highlighted the dynamic and often unpredictable nature of observational astronomy, where empirical data continuously challenge and refine theoretical models.

Looking forward, the methods refined in this lab, particularly in image processing and flux measurement, will enhance our capabilities in observing and analyzing other celestial bodies. Continued advancements in computational models and observational technologies hopefully promise to further our understanding of the cosmos, demonstrating the ongoing value of detailed empirical research in astronomy.

6 Acknowledgements

I would like to take the time to thank my lab partners, Kobe Bilstad and Brianna Peck, for their persistent efforts in this lab, making major efforts in sourcing the optimal Python libraries and modules to bring our lab results to fruition, along with other strong efforts in various other aspects of this lab. We were able to effectively coordinate our availabilities to spend as much time as possible working on this lab together, to ensure that our efforts were up to par with each other. I would also like to thank professors Jessica Lu and Alan Chew for their excellent advice and guidance throughout this lab, and the Astronomy Department at UC Berkeley for providing us with such an enriching lab experience. Finally, thank you to the reader of this report, I hope that I was able to concisely communicate and portray my lab results to you.

7 Appendix

7.1 Calculated Physical Parameters

Radii

- R_{star}: $9.71 \times 10^8 \pm 0.217 \times 10^8$ m
- R_{planet}: $1.01 \times 10^8 \pm 0.059 \times 10^8$ m

Masses

- M_{planet}: $1.75 \times 10^{27} \pm 0.514 \times 10^{27}$ kg

Volumes and Densities

- V_{planet}: $4.39 \times 10^{24} \pm 0.487 \times 10^{24}$ m^3
- ρ_{planet}: 370 ± 90.5 kg/m^3

Orbital Characteristics

- a: 0.0513 ± 0.0012 AU
- i: $83.37 \pm 0.65°$
- P_{orb}: 13773 ± 0.225 s
- v_{orb}: 2.09 ± 0.02 km/s

7.2 Observables

- T: 147.9 ± 0 mins
- τ_1: 45 ± 0 mins
- τ_2: 45 ± 0 mins
- δ: $0.08\% \pm 0\%$

7.3 Equations

Star Radius

$$R_{\text{star}} = R_{\text{sun}} \times 1.396$$
$$R_{\text{star, upper}} = R_{\text{sun}} \times (1.396 + 0.049)$$
$$R_{\text{star, lower}} = R_{\text{sun}} \times (1.396 - 0.043)$$

Describes the radius of the star, with upper and lower bounds.

Planet Radius

$$R_{\text{planet}} = \sqrt{\delta} \times R_{\text{star}}$$
$$R_{\text{planet, upper}} = \sqrt{\delta_{\text{upper}}} \times R_{\text{star, upper}}$$
$$R_{\text{planet, lower}} = \sqrt{\delta_{\text{upper}}} \times R_{\text{star, lower}}$$

Relates the planet's radius to observed transit depth and stellar radius.

Planet Volume

$$V_{\text{planet}} = \frac{4}{3}\pi R^3_{\text{planet}}$$
$$V_{\text{planet, upper}} = \frac{4}{3}\pi R^3_{\text{planet, upper}}$$
$$V_{\text{planet, lower}} = \frac{4}{3}\pi R^3_{\text{planet, lower}}$$

Calculates the volume of the planet with bounds.

Planet Density

$$\rho_{\text{planet}} = \frac{M_{\text{planet}}}{V_{\text{planet}}}$$
$$\rho_{\text{planet, upper}} = \frac{M_{\text{planet, upper}}}{V_{\text{planet, lower}}}$$
$$\rho_{\text{planet, lower}} = \frac{M_{\text{planet, lower}}}{V_{\text{planet, upper}}}$$

Determines the density of the planet, in $\frac{\text{kg}}{\text{m}^3}$.

NOTE: The following equations describe the orbital velocity depending on either the Transit Duration or Egress/Ingress duration. Transit calculations are more reliable since we had to approximate ingress duration, and thus set eccentricity.

Orbital Velocity (Egress)

$$v_{\text{orbital, egress}} = \frac{2 \times R_{\text{planet}}}{\tau}$$

$$v_{\text{orbital, upper egress}} = \frac{2 \times R_{\text{planet, upper}}}{\tau}$$

$$v_{\text{orbital, lower egress}} = \frac{2 \times R_{\text{planet, lower}}}{\tau}$$

Defines the speed at which the planet travels in its orbit based on the ingress/egress duration.

Orbital Velocity (Transit)

$$v_{\text{orbital, transit}} = \frac{2 \times R_{\text{star}}}{\mathrm{T}}$$

$$v_{\text{orbital, upper transit}} = \frac{2 \times R_{\text{star, upper}}}{\mathrm{T}}$$

$$v_{\text{orbital, lower transit}} = \frac{2 \times R_{\text{star, lower}}}{\mathrm{T}}$$

Defines the speed at which the planet travels in its orbit based on the transit duration.

Transit Angle

$$\psi_{\text{transit}} = \arcsin\left(\frac{\mathrm{T} \times v_{\text{orbital transit}}}{2 \times R_{\text{star}}}\right)$$

$$\psi_{\text{transit, upper}} = \arcsin\left(\frac{\mathrm{T} \times v_{\text{orbital, upper transit}}}{2 \times R_{\text{star, lower}}}\right)$$

$$\psi_{\text{transit, lower}} = \arcsin\left(\frac{\mathrm{T} \times v_{\text{orbital, upper transit}}}{2 \times R_{\text{star, lower}}}\right)$$

Calculates the angle ψ during transit.

Impact Parameter

$$b_{\text{transit}} = \cos(\psi_{\text{transit}})$$

$$b_{\text{transit, upper}} = \cos(\psi_{\text{transit, upper}})$$

$$b_{\text{transit, lower}} = \cos(\psi_{\text{transit, lower}})$$

Impact parameter b derived from ψ during transit.

Orbital Period

$$P_{\text{transit}} = \frac{2\pi \times R_{\text{star}}}{v_{\text{orbital transit}}}$$

$$P_{\text{transit, upper}} = \frac{2\pi \times R_{\text{star, upper}}}{v_{\text{orbital, lower transit}}}$$

$$P_{\text{transit, lower}} = \frac{2\pi \times R_{\text{star, lower}}}{v_{\text{orbital, upper transit}}}$$

Calculates the time of one orbit around the star.

Semi-Major Axis

$$a = \frac{v_{\text{orbital, transit}} \times P_{\text{transit}}}{2\pi}$$

$$a_{\text{upper}} = \frac{v_{\text{orbital, upper transit}} \times P_{\text{transit, upper}}}{2\pi}$$

$$a_{\text{lower}} = \frac{v_{\text{orbital, lower transit}} \times P_{\text{transit, lower}}}{2\pi}$$

The semi-major axis, determined from transit velocity and period.

Inclination

$$i_{\text{transit}} = \arccos\left(\frac{b_{\text{transit}} \times \left(R_{\text{star}} + R_{\text{planet}}\right)}{a}\right)$$

The angle by which the star system of interest is inclined relative to an observer.

Star Mass

$$M_{\text{star, transit}} = \frac{a^3(4\pi^2)}{G \times P^2_{\text{transit}}}$$

$$M_{\text{star, upper transit}} = \frac{a^3(4\pi^2)}{G \times P^2_{\text{upper transit}}}$$

$$M_{\text{star, lower transit}} = \frac{a^3(4\pi^2)}{G \times P^2_{\text{lower transit}}}$$

Calculates mass of the star during transit from semi-major axis and period.

References

[1] "AladinLite." Aladin/SIMBAD/Gaia DR 3/2MASS.

[2] European Space Agency. *Exoplanets in the Spotlight*. Available at: https://www.esa.int/Science_Exploration/Space_Science/Exoplanets/Exoplanets_in_the_spotlight

[3] Jensen, Eric. "Airmass Plot for TOI-2154 b on 2024-10-17." Swarthmore Transit Finder, NASA, https://astro.swarthmore.edu/transits/plot_airmass.cgi?observatory_string=37.343333%3B-121.636667%3BPST8PDT%3BLick%20Observatory&observatory_latitude=37.343333&observatory_longitude=-121.636667&target=TOI-2154%20b&ra=04:44:06.76&dec=+84:21:51.35&timezone=PST8PDT&jd=2460601.59896557&jd_start=10601.698&jd_end=10601.803&use_utc=0&max_airmass=2.4. Accessed 7 Nov. 2024.

[4] Jensen, Eric. "Find Exoplanet Transits." Edited by Alice Allen. NASA Exoplanet Archive Database.

[5] Jensen, Eric. "What to Observe." NASA, NASA, 5 Nov. 2024, https://exoplanets.nasa.gov/exoplanet-watch/latest-targets/.

[6] "NASA Exoplanet Archive - TOI-2154 Overview." NASA Exoplanet Archive, California Institute of Technology, https://exoplanetarchive.ipac.caltech.edu/overview/TOI-2154. Accessed 7 Nov. 2024.

[7] Rodriguez, Joseph E., et al. "Another shipment of six short-period giant planets from tess." Monthly Notices of the Royal Astronomical Society, vol. 521, no. 2, 28 Feb. 2023, pp. 2765–2785, https://doi.org/10.1093/mnras/stad595.

[8] Wesson, Roger. "Astronomical Object Visibility Plotter - TOI-2154," English, Nebulous Research, *airmass.org/*. Accessed 7 Nov. 2024.